IEICE TRANS. ELECTRON., VOL.E88–C, NO.2 FEBRUARY 2005

PAPER

Improved Boundary Element Method for Fast 3-D Interconnect Resistance Extraction*

Xiren WANG[†a)], ***Student Member***, **Deyan LIU**[††], **Wenjian YU**[†], ***and*** **Zeyi WANG**[†], ***Nonmembers***

SUMMARY Efficient extraction of interconnect parasitic parameters has become very important for present deep submicron designs. In this paper, the improved boundary element method (BEM) is presented for 3-D interconnect resistance extraction. The BEM is accelerated by the recently proposed quasi-multiple medium (QMM) technology, which quasi-cuts the calculated region to enlarge the sparsity of the overall coefficient matrix to solve. An un-average quasi-cutting scheme for QMM, advanced nonuniform element partition and technique of employing the linear element for some special surfaces are proposed. These improvements considerably condense the computational resource of the QMM-based BEM without loss of accuracy. Experiments on actual layout cases show that the presented method is several hundred to several thousand times faster than the well-known commercial software Raphael, while preserving the high accuracy.

key words: *interconnect resistance, fast extraction, improved boundary element method*

1. Introduction

Today, the deep submicron process technology is widely used. The parasitic parameters of interconnect wires, such as resistance and capacitance, have become important factors that govern the circuit delay and power consumption, etc [1], [2]. Fast and accurate resistance extraction is necessary for high-performance VLSI designs.

Some methods for resistance extraction have been published, such as the analytical method, the heuristic methods and numerical methods based on solving the Laplace equation [3]. The analytical formula $R = \rho L/S$ is exact only for very simple structures. The heuristic methods are not able to handle complex structures [4], and less accurate than numerical methods [5], [6]. Some 2-D numerical methods with higher accuracy have been published. They include the finite difference method (FDM) [7], finite element method (FEM) [8] and boundary element method (BEM) [3], [9]. Among them, BEM, with the advantage of fewer variables and better accuracy, has been successfully applied to the area of 3-D capacitance extraction [2], [10].

Manuscript received June 21, 2004.
Manuscript revised August 25, 2004.

[†]The authors are with Dept. Computer Science & Technology, Tsinghua Univ., Beijing 100084, China.
[††]The author is with Dept. Computer Engineering, UCSC, Santa Cruz, CA 95064 USA.

*This work is supported by the China National Science Foundation under Grant 90407004 and 60401010. Also, it is partly supported by National High Technology Research and Development Program of China (No. 2004AA1Z1050).

a) E-mail: wxr01@mails.tsinghua.edu.cn

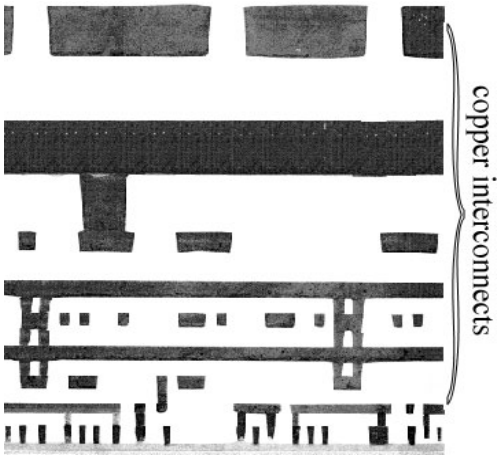

Fig. 1 Cross section of an 8-layer interconnect structure [1].

Currently, there are usually six to eight layers of interconnect wires in VLSI circuits, and they are connected by lots of vias between different layers. The spatial structure of the interconnects is becoming more and more complex. Fig. 1 gives an example from actual layouts [1]. For such structures, two-dimensional (2-D) numerical method for resistance extraction may be very inaccurate, due to lack of consideration of 3-D effects occurring at the corners of the crossing lines [11]. Moreover, in present deep submicron process technology, the resistivity of narrow wires is not constant for different wire widths or lengths [12], which makes it more difficult for 2-D methods to handle the actual structures. Therefore, the 3-D numerical method for resistance extraction becomes very important, which gives accurate result even for complex interconnect structures.

In this paper, we present a 3-D method for resistance extraction, under the electrostatic model. Our method calculates the direct current (DC) resistance, which is sufficiently accurate for some applications, such as time delay analysis [13]. Furthermore, under current process technology and circuit frequency the value of DC resistance is actually very close to that of the frequency-dependent resistance. More discussion is presented in Appendix A.

Our method is based on 3-D BEM and improved by the quasi-multiple medium (QMM) method. The QMM method is a recently proposed accelerating technique for BEM, and has been successfully applied in the 3-D capacitance extraction [2]. However, because of the difference between the simulation regions of the capacitance and resistance, how to

achieve highly-efficient resistance extraction with the QMM method becomes a problem. In this paper, we propose a scheme for region decomposition, an advanced non-uniform element partition scheme, and a technique to replace constant elements with linear elements for some sub-regions. These measures improve the 3-D BEM by reducing the variable number and enhancing the accuracy. Numerical experiments on actual interconnect structures show that the improved BEM consumes much less computational resource than the commercial software Raphael, but preserves higher accuracy.

The paper is organized as follows. Section 2 gives the principle of interconnect resistance calculation and its realization using BEM. Section 3 presents the scheme for region decomposition in the QMM-based BEM for 3-D resistance extraction. The other two improvements follow in Section 4. Then, the overall efficiency of our improved BEM is demonstrated with some numerical results. In the last section, there are some conclusions.

2. Interconnect Resistance Calculation

Usually, actual interconnect structures are with multiple terminals. We will firstly introduce the fundamental of resistance extraction, and then present its realization using boundary element method.

2.1 Resistance of Multi-Terminal Regions

In a region constituted by several conductors and multiple terminals, there is a resistor between each pair of terminals. A 2-D region and its equivalent resistance network are shown in Fig. 2.

To get the resistance values, we let the voltage of terminal j in the region be 1V and voltages of the other terminals be 0V. Then R_{jk}, the resistance between terminals j and k ($k \neq j$), is:

$$\frac{1}{R_{jk}} = \int_{\Gamma_{uk}} \sigma \cdot \frac{\partial u}{\partial n}\, d\Gamma = \int_{\Gamma_{uk}} \sigma \cdot q\, d\Gamma, \tag{1}$$

where Γ_{uk} is the boundary of terminal k, σ is the conductivity (reciprocal of resistivity), u is the electric potential and q is its normal derivative [3]. Repeating with different bias voltages, we can get the resistance matrix.

The q in (1) can be directly obtained using the boundary element method, and then we can get the resistances.

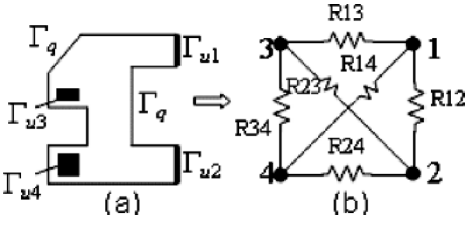

Fig. 2 A 2-D conductor region (a), and its equivalent resistance network (b). Γ_{uk} ($k = 1, \cdots, 4$) denotes terminals.

2.2 Numerical Resistance Extraction Using BEM

In order to get the q distribution within a homogeneous region, i.e. with single resistivity, it is accurate to formulate the region in terms of the Laplace equation

$$\frac{\partial^2 u}{\partial x^2} + \frac{\partial^2 u}{\partial y^2} + \frac{\partial^2 u}{\partial z^2} = 0 \tag{2}$$

with mixed boundary conditions (see (A· 1) in Appendix B), where u is the electric potential. If the region is with several different resistivities, it can be regarded as the set of smaller homogeneous regions. Such a problem is called a multi-region one. In each smaller region Ω_i, the electric potential u fulfills the above Laplace equation; on the interface of two adjacent regions a and b, u and q fulfill [2]

$$u_a = u_b, \quad \sigma_a \cdot \frac{\partial u_a}{\partial \boldsymbol{n_a}} = -\sigma_b \cdot \frac{\partial u_b}{\partial \boldsymbol{n_b}}, \tag{3}$$

where σ_a and σ_b are the conductivities of conductors a and b, and $\boldsymbol{n_a}$ and $\boldsymbol{n_b}$ are their unit normal vector. Thus BEM can handle very complex structures.

With the Green's identity and using the free-space Green's function as the weighting function, the Laplace equation (2) can be transformed into a direct boundary integral equation (BIE). After discretizing the region boundary into quadrilateral elements, we get the discretized BIE [3]

$$c_s u_s + \sum_{j=0}^{N_i-1} \int_{\Gamma_{ij}} q^* u\, d\Gamma = \sum_{j=0}^{N_i-1} \int_{\Gamma_{ij}} u^* q\, d\Gamma. \tag{4}$$

where c_s is a constant depending on the geometry around the collocation point s, u_s is the electric potential at point s, u^* is fundamental solution of Laplace equation and q^* is its normal derivative. The entire boundary of region Ω_i is Γ_i, and it is partitioned into N_i elements denoted by Γ_{ij}. Employing constant or linear elements (assuming variance occurs along x axis), we get the electric potential on Γ_{ij}:

$$u_{ij} = \begin{cases} u_{(00)}, & \text{for constant elements,} \\ u_{(11)}x + u_{(10)}, & \text{for linear elements,} \end{cases} \tag{5}$$

where $u_{(00)}$, $u_{(10)}$ and $u_{(11)}$ are unknown constants. Substituting (5) into (4) and utilizing the boundary conditions (and the interface conditions (3) for multi-region problems), we get a linear system

$$\boldsymbol{Ax} = \boldsymbol{f}, \tag{6}$$

where the variable vector $\boldsymbol{x}$ is composed of discrete$u$ and q unknowns. Solving this linear system, we can directly get q values, and then the resistance values through (1).

The non-symmetric matrix $\boldsymbol{A}$ in (6) is dense for a one-region problem, and is typically sparse for a multi-region problem. A preconditioned GMRES algorithm [14] is used to solve it efficiently.

3. Quasi-Multiple Medium Algorithm to Improve BEM

When the calculated region is complex and large, BEM becomes very slow, because a great number of variables are needed to get proper accuracy. Usually, it takes most of the time to generate and solve the linear system (6). If the generation and solution operations are accelerated, BEM will be more efficient. In interconnect capacitance extraction, an accelerating algorithm called quasi-multiple medium (QMM) was reported [2], [10]. Through averagely cutting mediums into fictitious parts, QMM can enhance the sparseness of $\boldsymbol{A}$ in (6) and speed up the generation and solution.

3.1 Basic Idea of Quasi-Multiple Medium Algorithm

We can see from (4) that it is only the same region's boundary elements (and the u or q unknowns on them) that have direct interactions, which means their coefficients in matrix $\boldsymbol{A}$ in (6) are not zero. Therefore, if an original homogeneous region is cut into fictitious sub-regions, matrix $\boldsymbol{A}$ turns from dense to sparse. For an original multi-region problem, $\boldsymbol{A}$ has a higher sparsity after quasi-cutting, because each sub-region contains fewer variables. Then it is possible that the generation and the solution of the linear system (6) are accelerated.

In a word, with a proper decomposition of the original region, QMM is able to speed up BEM calculation. On the other hand, quasi-cutting creates additional fictitious interfaces, which will bring additional variables and counteract the speed-up introduced by the higher sparsity of $\boldsymbol{A}$.

The QMM has been successfully applied to 3-D capacitance extraction [2], [10]. For 3-D resistance extraction, some specific techniques of QMM based BEM need to be investigated, because the simulation region and structure has large difference with that in capacitance extraction. In the following text, we will present a practical scheme of QMM for 3-D resistance extraction.

3.2 Practical Quasi-Cutting Scheme for QMM

There are roughly two ways to quasi-cut an original region, averagely and un-averagely. In the average scheme, after quasi-cutting, the lengths, widths or heights of the produced sub-regions are equal. The scheme is easier, and is applied in capacitance extraction [2], [10]. In resistance extraction, we find out by experiment that the un-average scheme is superior.

The un-averagely cutting scheme is based on the following: at low voltage frequency, the density of current flowing through corner sections of an interconnect wire is not uniform, but it becomes nearly uniform some distance (equaling the wire width at most) away from the corners [15]. We will separate the different sections with uniform or non-uniform current density, called cutting. By experiment, we find out that when the cutting distance D equals 0.5 times of the conductor width, the scheme is very efficient. We employ this value from now on.

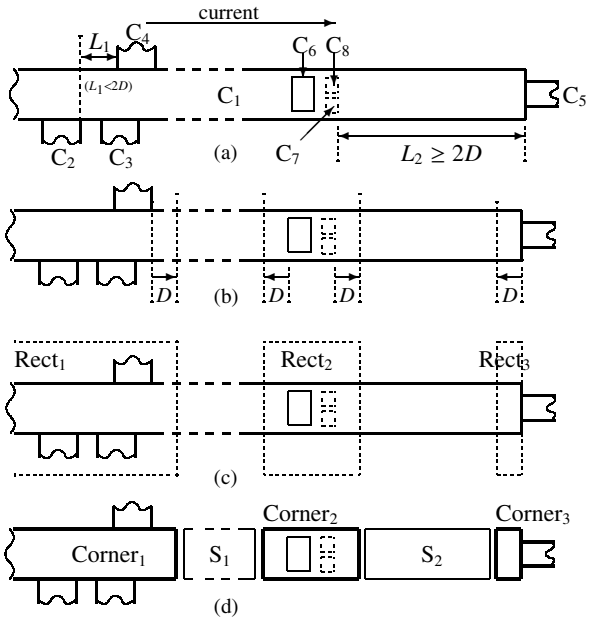

Fig. 3 Four steps of the un-averagely Quasi-cutting scheme. Conductor C_1 will be cut along the horizontal direction. (a) Identify interfaces between conductors. (b) Extend the interface polygons horizontally by a distance of D, to the left and to the right. Overlapping lines are omitted for better visibility. (c) Combine all little polygons into $Rect_1$ to $Rect_3$. (d) Cut each of these rectangles as a whole respectively, producing corner conductors ($Corner_1$, $Corner_2$ and $Corner_3$) and straight ones (S_1 and S_2).

There are four steps to cut a conductor. Firstly, identify the interfaces between the conductor to be cut and other conductors. Secondly, extend the interface polygons by D in the current flow direction and the reversed direction. Thirdly, combine all the polygons, and get some large enough rectangles. Lastly, cut each of the rectangles as a whole from the original conductor, separately. The sub-conductors containing the rectangles are called *corner conductors*, and the others are *straight conductors*. Note that the straight conductor may be very long.

For example, in Fig. 3, to make the description simple, assume that conductor C_1 is to be cut and current flows horizontally. C_2 to C_5 are in the same plane as C_1. C_6 is above C_1. C_7 and C_8 is below C_1. The cutting process is like (a) to (d). Finally, C_1 is cut into three corner sub-conductors ($Corner_1$, $Corner_2$ and $Corner_3$), and two straight ones (S_1 and S_2).

3.3 Experiment on QMM Algorithm

In the following text, in order to examine the performance of the presented QBEM (QMM accelerated BEM), we compare it with pure BEM (without improvements), and with the well-known commercial software Raphael RC3 (version 2000.2, a finite difference solver with advanced non-uniform meshes) [16]. Two test cases from actual layouts are used throughout this paper. They are within smallest cubes of

$1.83 \times 2.67 \times 1.50\,\mu m^3$ and of $10.33 \times 9.55 \times 8.45\,\mu m^3$, respectively. There are two layers of wires with different resistivities in case 1, and three layers of wires in case 2 (the latter is shown in Fig. 4). All programs run on Sun Ultra Enterprise 450 (CPU frequency 248 MHz). The results of them are resistance matrixes, corresponding to the network in Fig. 2. In all the coming tables, "GridNum" is the default element number for BEM (or the default grid number for Raphael), and "Time" means default running time. "Error" means the maximum of the absolute diagonal values in the error matrices, where the criteria compared with are the results of Raphael RC3 using denser meshes of 2×10^6 grids and 4×10^6 grids, respectively.

For the two cases, results of QBEM with the un-average or average scheme† are shown in Table 1. Results of pure BEM and Raphael are also listed. "RegnNum" in the table means the number of sub-regions.

The table shows that the BEM without improvement is also much faster than Raphael which is based on finite difference method, but has a worse accuracy. QBEM with either cutting scheme occupies less computational resource than BEM, that is to say, QMM is able to improve BEM calculation.

Note that QBEM with the un-average scheme here has a smaller number of sub-regions and boundary elements than with the average scheme. The reason is that in the un-average scheme, even if a straight conductor is very long, it is not cut any more. This may restrict the accelerating effect of the QMM. However, in Section 4.4.3 we will learn that it is much better to employ linear elements for such a straight conductor than to cut it into more parts and then partition the traditional constant elements.

It is also noted that errors of QMM are larger than those of the pure BEM. Generally speaking, the mesh discretization error is the major source of the numerical errors for BEM computation [17]. Although the QMM dose not bring new source of error, the more complex sub-regions after quasi-cutting make the boundary element mesh less reasonable. Therefore, the QMM accelerated BEM reveals less accuracy. The nonuniform meshes and linear boundary elements in the following Section IV will enhance the accuracy.

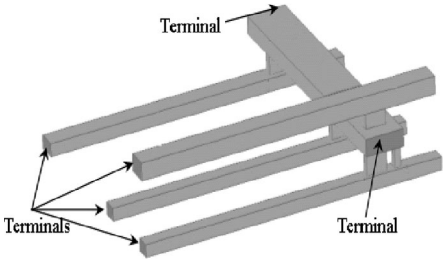

Fig. 4 The second test case. There are three layers of wires which are with different resistivity values in it.

4. Nonuniform Meshes and Linear Boundary Elements

When the above un-average scheme is used, the original region becomes a set of sub-regions which are very likely to be of different electrical properties. For example, they may be equipotential bodies or straight conductors with uniform current density. We can make use of the difference. We will select dense or sparse element meshes according to the current variation. For straight conductors, one linear element can replace many constant elements.

4.1 Discard Conductors not in Current Flow Paths

As we know, if a conductor is not in the current flow path within the calculated region, it is equipotential everywhere. Such a conductor is of no use for numerical calculation for resistance. Removing†† it from the calculated region affects neither the current nor the resistance values, but is able to reduce the element and variable number. In other words, we partition zero element on it.

For example, after quasi-cutting with the above un-average scheme, conductor W in Fig. 5(a) can be discarded, and the leftover region in Fig. 5(b) is smaller.

4.2 Partition Elements More Accurately

Usually, boundary elements are divided in two perpendicular directions on a surface, as that in capacitance extraction [2]. In resistance extraction, some conductor surfaces needs to be partitioned in both directions, while others only in one direction without sacrificing accuracy.

Take the straight conductor segment in Fig. 6 as an example. Because of the regularity of the conductor geometry, the current is supposed to distribute nearly uniformly across

†Here, the average scheme is to cut the original conductors averagely into sub parts whose lengths are less than r times of conductor width. The performance of QBEM with the scheme varies with the r value. When $r = 2$, the performance will be relatively high.

††Removing here does not means really getting rid of them from the original region. They are just temporarily neglected in the numerical calculation for resistance.

Table 1 QBEM with the un-average scheme and average scheme.

	Case 1						Case 2					
	RegnNum	GridNum	Mem(MB)	Time(s)	Error(%)	Speedup	RegnNum	GridNum	Mem(MB)	Time(s)	Error(%)	Speedup
QBEM(Un-Avg)	12	839	0.52	2.46	5.22	157.7	25	4276	9.94	80.55	3.71	76.0
QBEM(Avg)	24	870	0.51	1.85	5.47	209.7	56	4639	8.22	49.01	5.28	124.8
Pure BEM	9	835	0.68	3.79	4.40	102.4	12	4536	17.08	154.65	2.62	39.6
Raphael RC3	-	63168	14.00	388.03	1.05	1	-	336398	89.00	6118.76	1.61	1

the cross section. Therefore in Fig. 6(a), the potential distribution on element e_1 and e_2 is the same. We do not need to sperate them while making discretization. For this reason, the four side surfaces of the straight conductor can only be partitioned in one direction (like that shown in Fig. 6(b)), without loss of accuracy.

It is also possible that some surfaces on corner conductors can be divided in only one direction. For example, in Fig. 7, we can predict that the current flows horizontally above the bottom surface of conductor B. Since this surface is relatively remote from the conductor connection portion and the current near it is nearly uniformed, the elements on it can be divided only in one direction (shown with the dashed lines in Fig. 7).

It can be expected that the mixed-direction scheme is able to reduce the element number. For the above two test cases, the results of QBEM with the mixed-direction scheme and with the usual two-direction scheme are shown in Table 2.

This table verifies that the mixed-direction scheme can really reduce the element number, and condense computational resource usage. And the error is reduced for both cases. This is because that the new element meshes approximate actual current distribution much better.

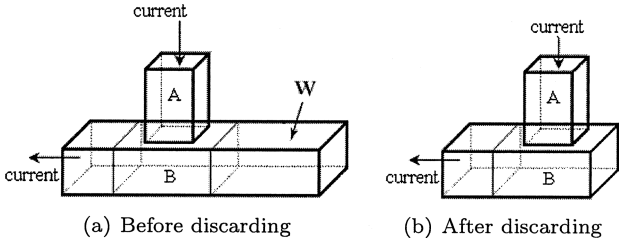

Fig. 5 Discarding the waste conductor W.

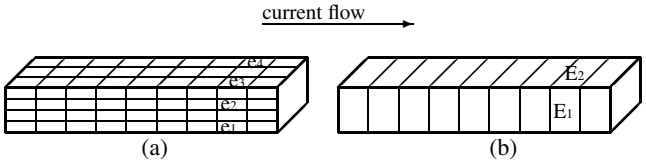

Fig. 6 Divide elements on a straight conductor in both directions and in only one direction. Assume that current flows horizontally. (a) In both directions. (b) In one direction.

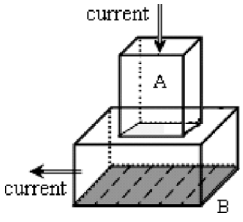

Fig. 7 Current flows downwards, and turns to the left. The current flows horizontally above the bottom surface (in grey) of conductor B. The elements are divided horizontally, as separated by dashed lines.

4.3 Employ Linear Elements for Straight Conductors

Recalling the WHOLE scheme in section 3.3.2, the current flowing through a straight conductor will be uniform (or nearly uniform), and thus the electric potential on its surfaces will vary linearly along the current path. In other words, if the current in the conductor flows along the x axis, the potential on its one surface is a linear function

$$u = u_1 x + u_0, \tag{7}$$

where u_1 and u_0 are unknown constants. Then, we can employ linear element to accurately simulate the linear potential u. In this way, many constant elements on this surface are replaced by one linear element.

For a constant element, there is only one unknown. We select the element center as the collocation point to get the BIE equation (4). For a linear element, there are two unknowns, like u_1 and u_0 in (7). We select two collocation points from the element, and then the variable number and the equation number are balanced. We will discuss how to generate the equations in Appendix B.

With linear elements employed for straight conductors and constant elements for the other conductors, the new QBEM is called a coupling QBEM[†]. For a line conductor ($1 \times 10 \times 1\,\mu\text{m}^3$ in size, resistivity is 1Ωm) with terminals at two far ends, there are only four linear elements and two constant elements in the coupling QBEM. The resistance value obtained by QBEM is $10.00002\,\text{K}\Omega$, while the analytical value is $10\,\text{K}\Omega$. For the two test cases, Table 3 shows the results of the coupling QBEM and constant QBEM (with only constant elements).

From the table we find out that the coupling QBEM has much fewer elements, because one linear element can replace many constant ones. The coupling QBEM takes up much less time or memory than any QBEM in the above text or pure BEM. Besides, it has a higher accuracy. In order to get the accelerating effects introduced by linear elements, we prefer to obtain long straight conductors when quasi-cut the original region. This is why we don't cut straight conductors any more in the un-averagely cutting scheme in section 3.

[†]It applies the un-average scheme to cut the original region. With this scheme, straight conductors are easier to be identified.

Table 2 QBEM with the mixed-directions and two-direction scheme.

	Case 1					Case 2				
	GridNum	Mem(MB)	Time(s)	Error(%)	Speedup	GridNum	Mem(MB)	Time(s)	Error(%)	Speedup
QBEM(mixed-dir)	587	0.19	1.03	1.85	376.7	3233	5.48	29.25	2.06	209.2
QBEM(two-dir)	870	0.51	1.85	5.47	209.7	4639	8.22	49.01	5.28	124.8
Raphael RC3	63168	14.00	388.03	1.05	1	336398	89.00	6118.76	1.61	1

Table 3 QBEM with constant-linear elements and pure constant elements.

	Case 1					Case 2				
	GridNum	Mem(MB)	Time(s)	Error(%)	Speedup	GridNum	Mem(MB)	Time(s)	Error(%)	Speedup
QBEM(Coupling)	287	0.10	0.53	0.67	732.1	1173	1.52	10.0	−1.05	611.9
QBEM(constant)	870	0.51	1.85	5.47	209.7	4639	8.22	49.01	5.28	124.8
Raphael RC3	63168	14.00	388.03	1.05	1	336398	89.00	6118.76	1.61	1

Table 4 Combination of all improvements.

	Case 1					Case 2				
	GridNum	Mem(MB)	Time(s)	Error(%)	Speedup	GridNum	Mem(MB)	Time(s)	Error(%)	Speedup
QBEM	230	<0.10	0.44	0.79	**881.9**	598	0.43	2.78	−1.01	**2201.0**
Pure BEM	835	0.68	3.79	4.40	**102.4**	4536	17.08	154.65	2.62	**39.6**
Raphael RC3	63168	14.00	388.03	1.05	**1**	336398	89.00	6118.76	1.61	**1**

5. Overall Numerical Results

Applying the QMM algorithm in Section 3, the non-uniform meshes and linear elements in Section 4, and we get the final QBEM. Run the test cases using this QBEM, the pure BEM and Raphael RC3, respectively. The computational results are listed in Table 4.

Compared with the data in Table 3, the CPU times of QBEM are reduced further in Table 4. This is because here the techniques of discarding conductor not in current path and partitioning element in only one direction are combined, which result in the further reduction of boundary elements.

Table 4 shows that the computational resources occupied by the pure BEM is several to hundreds of times more than the final QBEM, but the errors are larger. One reason is that the constant element meshes and the linear elements in the final QBEM can more accurately reflect the physical current distribution in the simulation region. Compared with Raphael with default meshes, the final QBEM is hundreds of to thousands of times faster, saves most of memory, and achieves comparable or higher accuracy.

6. Conclusions

In this paper, we present the boundary element method applied to 3-D interconnect resistance calculation and improve it by the improved quasi-multiple medium (QMM) method. An un-average quasi-cutting scheme is proposed for QMM, and two related techniques are also presented to make the element meshes more reasonable. One is the nonuniform element meshes which can reduce the element number and enhance the accuracy. The other is coupling the linear elements for straight conductors, which represents the linear electric potential variance. Experiments on actual layout cases show that these improvements can considerably enhance the efficiency of BEM calculation, but not sacrifice accuracy. When compared with the well-known software Raphael, the final improved BEM runs hundreds of to thousands of times faster, consumes much less memory and preserves higher accuracy.

References

[1] A.S. Brown, "Fast films," IEEE Spectr., vol.40, no.2, pp.36–40, 2003.
[2] W. Yu, Z. Wang, and J. Gu, "Fast capacitance extraction of actual 3-D VLSI interconnects using quasi-multiple medium accelerated BEM," IEEE Trans. Microw. Theory Tech., vol.51, no.1, pp.109–119, 2003.
[3] Z. Wang and Q. Wu, "A two-dimensional resistance simulator using the boundary element method," IEEE Trans. Comput.-Aided Des. Integr. Circuits Syst., vol.11, no.4, pp.497–504, 1992.
[4] A.J. Kemp and J.A. Pretoriu, "The generation of a mesh for resistance calculation in intergrated circuits," IEEE Trans. Comput.-Aided Des. Integr. Circuits Syst., vol.7, no.10, pp.1029–1037, 1988.
[5] J.P. Hwang, "REX—A VLSI parasitic extraction tool for electromigration and signal analysis," ACM/IEEE Design Automation Conference, pp.717–722, 1991.
[6] L. Ladage and R. Leupers, "Resistance extraction using a routing algorithm," ACM/IEEE Design Automation Conference, pp.38–42, 1993.
[7] M. Glegharbour and J.M. Drake, "Calculation of multiterminal resistance in integrated circuits," IEEE Trans. Circuits Syst., vol.33, no.4, pp.462–465, 1986.
[8] T. Mitsuhashi and K. Yoshida, "A resistance calculation algorithm and its application to circuit extraction," IEEE Trans. Comput.-Aided Des. Integr. Circuits Syst., vol.16, no.3, pp.337–345, 1987.
[9] W. Sun, W. Hong, and W.W. Dai, "Resistance extraction using superconvergence accelerated boundary element method," Asia-Pacific Microwave Conference, vol.3, pp.1061–1064, 1997.
[10] W. Yu and Z. Wang, "Fast quasi-multiple medium method for 3-D BEM calculation of parasitic capacitance," Computers and Mathematics with Applications, vol.45, no.12, pp.1883–1894, 2003.
[11] K.M. Cham, S. Oh, J.L. Moll, K. Lee, P.V. Voorde, and D. Chin, Computer-Aided Design and VLSI Device Development, second ed. Cluwer Academic Publishers, Boston, 1988.
[12] F. Chen and D. Gardne, "Influence of line dimensions on the resistance of Cu interconnections," IEEE Electron Device Lett., vol.19, no.12, pp.508–510, 1998.
[13] Y. Cao, X. Huang, D. Sylvester, T. King, and C. Hu, "Impact of on-chip interconnect frequency-dependent R(f)L(f) on digital and RF design," IEEE International ASIC/SOC Conference, pp.438–442, 2002.
[14] Y. Saad and M.H. Schultz, "GMRES: A generalized minimal residual algorithm for solving nonsymmetric linear systems," SIAM J. Sci. Statis. Comput., vol.7, no.3, pp.856–869, 1986.
[15] A.J. Walton, R.J. Holwill, and J.M. Robertson, "Numerical simulation of resistive interconnects for integrated circuits," IEEE J. Solid-State Circuits, vol.20, no.6, pp.1252–1258, 1985.
[16] Avant! Corp., Raphael Reference Manual, 2000.

[17] Z. Zhao and X. Wang, "Error estimation and h adaptive boundary elements," Engineering Analysis with Boundary Elements, vol.23, no.10, pp.793–803, 1999.
[18] M. Kamon, M.J. Tsuk, and J.K. White, "FastHenry: A multipole-accelerated 3-D inductance extraction program," IEEE Trans. Microw. Theory Tech., vol.42, no.9, pp.1750–1758, 1994.
[19] W.T. Weeks, L.L. Wu, M.F. McAllister, and A. Singh, "Resistive and inductive skin effect in rectangular conductors," IBM J. Res. Dev., vol.23, no.6, pp.652–660, 1979.
[20] Semiconductor Industry Association, "International technology roadmap for semiconductors," 2001, [online]. Available: http://public.itrs.net/

Appendix A: Direct Current (DC) Resistance Can Be Accurate Enough for Narrow Wires at Present

Usually, the interconnect resistance value will increase with the operating frequency. The resistance can be called frequency-dependent resistance. It is paid much attention to, and some related algorithms were published, for example, FastHenry [18].

Generally speaking, at high frequency, frequency-dependent resistance is more suitable than DC resistance. However, due to the consideration of fairly comprehensive electromagnetic effects, the solution for frequency-dependent resistance will generally need a large number of unknowns and require a great deal of computational time. The DC resistance is much easier to be obtained, and we will see that the DC extraction is accurate enough in some cases.

In fact, the decrease in the feature size and wire width may enhance the accuracy of DC resistance. As we know, the resistance increases with frequency because of the skin effect, the proximity effect and so on. Here we only give a rough discussion about the skin effect in theory.

The skin depth is $\delta = 1/\sqrt{\pi f \mu \sigma}$, where f is the frequency, μ is the magnetic permeability, and σ is the conductivity [19]. ITRS'2001 forecasts that in 2007, the feature size will be $0.065\,\mu$m, and the clock frequency will be 6739 MHz [20]. At that time, the skin depth of copper wires is about $0.81\,\mu$m. Assume some local wires are with the aspect ratio (height/width) of 3. Then the skin depth is much larger than half width or half height of the minimum wires, i.e. $\delta \gg (0.065 \times 0.5)$, $\delta \gg (0.065 \times 0.5 \times 3 = 0.098)$. This indicates that the skin effect of narrow wires is too weak to change the uniform distribution of current in the wire cross sections. Therefore, the DC resistance value is able to be very approximate to the actual value in the near future. This is supported by FastHenry's results for some not very simple structures.

Of course, for global wires which have larger cross sections, the frequency-dependent resistance will be more suitable than DC resistance. The numerical extraction method presented in this paper is mainly oriented to local interconnects which are typically narrow wires.

Moreover, DC resistance is sufficiently accurate for some applications, such as time delay analysis [13].

In a word, the presented method for DC resistance extraction is reasonable, and useful at present and in the near future.

Appendix B: Integral Equations of Constant and Linear Boundary Elements

The detailed boundary conditions of (2) are

$$u = \bar{u}\ (\text{on}\ \Gamma_u),\ q = 0\ (\text{on}\ \Gamma_q), \tag{A·1}$$

where $\bar{u}$ is 1 or 0 (see Section 2), Γ_u is the boundary of terminals, and Γ_q is conductor boundary. The entire boundary Γ is $\Gamma_q + \Gamma_u$.

Here, let the entire boundary $\Gamma = \Gamma_{const} + \Gamma_{linear}$, where Γ_{const} is the boundary composed of constant element and Γ_{linear} is the boundary constituted by linear elements. If Γ_{linear} is an empty set, u or q on an element will be constant, and for a collocation point s, (4) is

$$c_s u_s + \sum_{j=0}^{N-1} \left(\int_{\Gamma_j} q^* d\Gamma \right) u_j = \int_{\Gamma} u q^* d\Gamma, \tag{A·2}$$

where the integral on constant elements can be obtained using the numerical integral or analytical integral (refer to [2]). On linear elements, u is a linear function like (7), and for point s, (4) becomes

$$\begin{aligned} c_s u_s \int_{\Gamma_{const}} u q^* d\Gamma + \sum_{lj=0}^{N_l-1} \left(\int_{\Gamma_{lj}} q^* \left(u_{lj}^1 x + u_{lj}^0 \right) d\Gamma \right) \\ = \int_{\Gamma_{linear}} u^* q d\Gamma + \int_{\Gamma_{const}} u^* q d\Gamma, \end{aligned} \tag{A·3}$$

where the first integral on constant elements has similar solution to that in (A·2), Γ_{lj} is the jth element of Γ_{linear}, N_l is the total number of Γ_{lj}, and u_{lj}^1 and u_{lj}^0 are unknown constants. Because the linear element in this paper is only on conductor surfaces where $q = 0$ (see (A·1)), $\int_{\Gamma_{linear}} u^* q d\Gamma = 0$. Therefore, in addition to the integrals on constant elements, here we only need to get the potential integral on a linear element Γ_l:

$$\begin{aligned} \text{IntU} &= \int_{\Gamma_l} q^* u d\Gamma = \int_{\Gamma_l} q^* (u_1 x + u_0) d\Gamma \\ &= \left(\int_{\Gamma_l} q^* x d\Gamma \right) u_1 + \left(\int_{\Gamma_l} q^* d\Gamma \right) u_0. \end{aligned} \tag{A·4}$$

Now, we need the coefficients of u_1 and u_0.

For a non-rectangle Γ_l, we can get the coefficients through numerical integral. If Γ_l is a rectangle (as shown in Fig. A·1), the coefficients can be numerically or analytically obtained. Here we select the analytical integral, and give the derivation of the equations.

In order to make the discussion simple, assume that the integral point (x, y, z) is in a horizontal plane $z = z_{int}$ with unit normal vector of $n = \{0, 0, 1\}$. Let the coordinate of the collocation point s be (x_s, y_s, z_s).

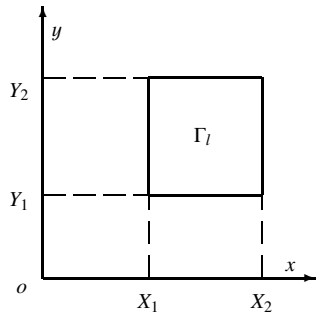

Fig. A· 1 Coordinate boundary of linear element Γ_l.

$$q^* = \frac{\partial u^*}{\partial n} = \nabla\left(\frac{1}{4\pi r}\right)\cdot n = -\frac{1}{4\pi r^2}\frac{\partial r}{\partial z}. \quad (A\cdot 5)$$

$$r = \sqrt{(x-x_s)^2+(y-y_s)^2+(z-z_s)^2},$$

$$\frac{\partial r}{\partial z} = \frac{z-z_s}{r}. \quad (A\cdot 6)$$

Substituting (A· 6) into (A· 5), we get

$$q^* = -\frac{z-z_s}{4\pi r^3} = \frac{Z}{4\pi r^3}, \quad (A\cdot 7)$$

where the constant Z is $z_s - z_{int}$. Therefore

$$\begin{aligned}\mathrm{IntU} &= \frac{Z}{4\pi}\left(\int_{\Gamma_l}\frac{x}{r^3}d\Gamma\right)\cdot u_1 + \frac{Z}{4\pi}\left(\int_{\Gamma_l}\frac{1}{r^3}d\Gamma\right)\cdot u_0 \\ &= \frac{Z}{4\pi}I_1\cdot u_1 + \frac{Z}{4\pi}I_2\cdot u_0, \end{aligned} \quad (A\cdot 8)$$

where

$$I_1 = \int_{\Gamma_l}\frac{x}{r^3}d\Gamma = \iint\frac{x}{r^3}dxdy \quad (A\cdot 9)$$

and

$$I_2 = \int_{\Gamma_l}\frac{1}{r^3}d\Gamma = \iint\frac{1}{r^3}dxdy. \quad (A\cdot 10)$$

We will only discuss the related indefinite integrals with the integral constant C omitted, and give entire equations at last. Let $R = \sqrt{x^2+y^2+Z^2}$. Consider I_1:

$$\begin{aligned} I_1 = \iint\frac{x}{r^3}dxdy &= \iint\frac{x'+x_s}{R^3}dx'dy \\ &= I_{11} + x_s I_{12}, \end{aligned} \quad (A\cdot 11)$$

where $I_{11} = \iint\frac{x}{R^3}dxdy$ and $I_{12} = \iint\frac{1}{R^3}dxdy$. Consider I_{12} in the two steps of I_{121} and I_{122}:

$$I_{121} = \int\frac{1}{R^3}dx = \frac{x}{(y^2+Z^2)R}, \quad (A\cdot 12)$$

and

$$\begin{aligned} I_{122} &= \int\frac{x}{(y^2+Z^2)R}dy \\ &= \frac{1}{Z}\arctan\left(\frac{x}{Z}\cdot\frac{y}{R}\right). \end{aligned} \quad (A\cdot 13)$$

Substituting (A· 12) and (A· 13), we can get I_{12}. Secondly, let

$$I_{11} = \iint\frac{x}{R^3}dxdy, \quad (A\cdot 14)$$

and we consider in two steps:

$$I_{111} = \int\frac{x}{R^3}dx = -\frac{1}{R} \quad (A\cdot 15)$$

and

$$I_{112} = \int\frac{1}{R}dy = \log(y+R). \quad (A\cdot 16)$$

Then I_{11} can be obtained. Obviously, I_2 has a similar solution to I_{12}.

Finally, we write the entire formulas of I_1 and I_2:

$$\begin{aligned} I_1 &= I_{11} + x_s I_{12} \\ &= \log\left(\frac{(y_2+\sqrt{x_1^2+y_2^2+Z^2})}{(y_2+\sqrt{x_2^2+y_2^2+Z^2})}\right) \\ &\quad + \log\left(\frac{(y_1+\sqrt{x_2^2+y_1^2+Z^2})}{(y_1+\sqrt{x_1^2+y_1^2+Z^2})}\right) \\ &\quad + \frac{x_s}{Z}\Bigg[\arctan\left(\frac{x_2y_2}{Z\sqrt{x_2^2+y_2^2+Z^2}}\right) \\ &\qquad + \arctan\left(\frac{x_1y_1}{Z\sqrt{x_1^2+y_1^2+Z^2}}\right) \\ &\qquad - \arctan\left(\frac{x_1y_2}{Z\sqrt{x_1^2+y_2^2+Z^2}}\right) \\ &\qquad - \arctan\left(\frac{x_2y_1}{Z\sqrt{x_2^2+y_1^2+Z^2}}\right)\Bigg], \end{aligned} \quad (A\cdot 17)$$

and

$$\begin{aligned} I_2 &= \frac{1}{Z}\Bigg[\arctan\left(\frac{X_2Y_2}{Z\sqrt{X_2^2+Y_2^2+Z^2}}\right) \\ &\quad + \arctan\left(\frac{X_1Y_1}{Z\sqrt{X_1^2+Y_1^2+Z^2}}\right) \\ &\quad - \arctan\left(\frac{X_1Y_2}{Z\sqrt{X_1^2+Y_2^2+Z^2}}\right) \\ &\quad - \arctan\left(\frac{X_2Y_1}{Z\sqrt{X_2^2+Y_1^2+Z^2}}\right)\Bigg], \end{aligned} \quad (A\cdot 18)$$

where $[X_1, X_2]$, $[Y_1, Y_2]$ are the boundary coordinates of the rectangle Γ_l (as shown in Fig. A· 1), $[x_1, x_2] = [X_1 - x_s, X_2 - x_s]$, $[y_1, y_2] = [Y_1 - y_s, Y_2 - y_s]$, and $Z = z_s - z_{int}$.

Xiren Wang received the B.S. degree from Xidian Univ., Xi'an, and Master degree in Computer Science from Tsinghua Univ., Beijing, China, in 2001 and 2003. At present, he is working towards the Ph.D. degree. His main research interests include interconnect resistance/capacitance extraction and simulation in VLSI circuits, substrate coupling analysis and modelling in mixed-signal circuits, and the direct boundary element methods application in electromagnet field analysis.

Deyan Liu received the B.S. degree in Electronic Engineering, M.S. degree in Computer Science from Tsinghua University, China, in 1999 and 2002. He is currently a graduate student in Computer Engineering in University of California at Santa Cruz, USA. His main research interest is CAD for VLSI, especially in interconnects resistance,capacitance and partial reluctance (K method) extraction.

Wenjian Yu received the B.S. and Ph.D. degrees in computer science from Tsinghua University, China, in 1999 and 2003, respectively, all with the highest honor. Since August 2003, he has been a Research Assistant in the Department of Computer Science and Technology at Tsinghua University. His research interests include the parasitic parameter extraction of interconnects in VLSI circuits, the direct boundary element analysis of electromagnetic field and modeling and simulation of VLSI interconnects. Dr. Yu was the Technical Program sub-Committee member of the ACM/IEEE Asia South-Pacific Design Automation Conference in 2005. He received the Microsoft Fellowship Award in 2002, and the distinguished Ph.D. Award from Tsinghua Univ. in 2003. He has served as a reviewer for IEEE Trans. on CAD, and published more than 30 technical papers in refereed journals or conferences.

Zeyi Wang graduated from the Department of Computational Mathematics in Xian Jiaotong University, Xian, China, in 1965. Since 1965, he has been with Tsinghua University, Beijing, China, where he is currently a professor with the Department of Computer Science and Technology. From 1987 to 1988, he was a visiting scholar at Stanford University working on 3-D device simulation on a parallel computer. His main research interests are the applications and research of the numerical methods, including the parallel computations in the areas of VLSI-CAD such as circuit analysis, device simulation and parasitic interconnect parameter extraction.